ELSEVIER

Computers and Geotechnics, Vol. 19, No. 1, pp. 1–22, 1996

0266-352X(95)00037-2 0266-352X/96 $15.00+0.00

Finite Element Analysis of Centrifuge Tests on Reinforced Embankments on Soft Clay

J. S. Sharma & M. D. Bolton

Cambridge University Engineering Department, Trumpington Street, Cambridge CB2 1PZ, U.K.

(Received 1 May 1995; revised version received 10 October 1995; accepted 17 October 1995)

ABSTRACT

The behaviour of reinforced embankments on soft clay has been explored using the technique of centrifuge modelling. Controlled in-flight embankment construction was carried out successfully in the centrifuge over a soft clay layer reinforced with an instrumented geotextile and the behaviour of the subsoil and the response of the reinforcement was observed. Analyses of idealized prototypes provided by the centrifuge tests have been carried out using the CRISP93 finite element program in which the stress-induced anisotropic behaviour of the one-dimensionally consolidated clay foundation was modelled. The results of the centrifuge model tests and their predictions using CRISP93 were in good agreement with each other. Also, the magnitude of tension induced in the reinforcement was found to be very sensitive to the magnitude and distribution of undrained shear strength of the clay foundation, indicating the importance of the effect of the anisotropy of the clay foundation on the behaviour of reinforced embankments. Copyright © 1996 Elsevier Science Ltd

INTRODUCTION

Quite often, e.g. while constructing motorways or permanent ways, there arises a need for the construction of embankments on soft clay. The lowest margin of safety of such embankments is at the end of construction when the loading is at its maximum whereas the strength of the soil is at its lowest due to development of excess pore pressures. Several techniques, such as staged construction, preloading and installation of wick drains, are available for enhancing the stability of these embankments. However, in recent years, many designers around the world are specifying base reinforcement as one of the solutions for the short-term instability (Fig. 1).

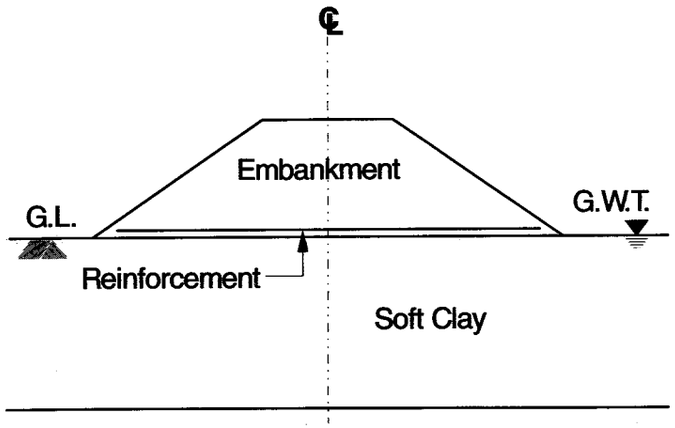

Fig. 1. Reinforced embankment on soft clay.

The idea behind this technique is to make use of the tensile strength of the reinforcement to limit the spreading of the embankment and lateral displacement of the clay foundation. Although this technique is widely used nowadays and data are available from detailed finite element analyses and instrumented field trials, the behaviour of reinforced embankments is far from clear. This paper describes an investigation into the behaviour of reinforced embankments on soft clay using the finite element method, comparing the results with those obtained from a series of centrifuge model tests.

CENTRIFUGE MODEL TESTING: PROCEDURE AND RESULTS

Centrifuge model testing, because of its ability to reproduce the same stress levels in a small-scale model as those present in a full-scale prototype, is a useful tool in the investigation of geotechnical problems. Idealized conditions may be created in centrifuge models to facilitate the validation of analytical or numerical solutions. In the present study, three 1:40 scale centrifuge model tests were performed using the Cambridge University 10 m balanced beam centrifuge [1]. Figure 2 shows the details of a typical centrifuge model. Due to inherent symmetry about the centreline, only one half of the structure was modelled. Table 1 gives a summary of each of the three centrifuge tests. These tests are described in detail by Sharma [2]. Hence, only a brief description of the equipment and testing method is provided here.

The speswhite kaolin clay was one-dimensionally consolidated to a maximum vertical pressure of 100 kPa. It was then trimmed to the dimensions of the model. A matrix of black plastic markers was installed on the front face of the clay block for the measurement of displacements using in-flight

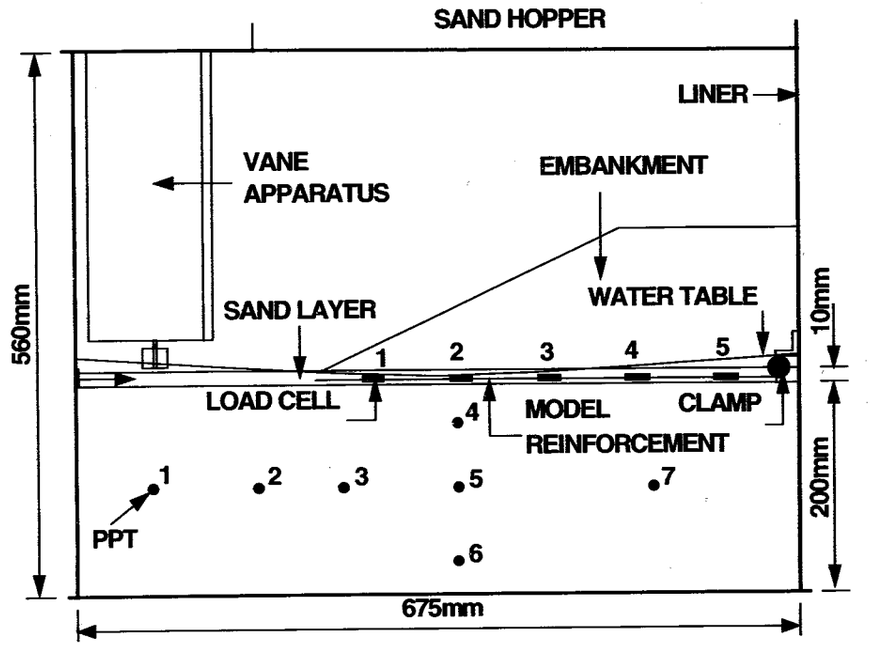

Fig. 2. Typical arrangement of centrifuge models.

TABLE 1
Details of the centrifuge tests

Test code	*Depth of clay*	*Type of reinforcement*
JSS7	200 mm	Geotextile
JSS8	200 mm	Unreinforced
JSS12	100 mm	Geotextile

photography. A polyester woven geotextile, having nominal tensile strength of 9.5 kN/m (380 kN/m at prototype scale) at 10% axial strain, was used as the model reinforcement. Five load cells, extending across the whole width, were constructed on this reinforcement for monitoring the tension in the reinforcement during centrifuge testing. These load cells were about 0.7 mm thick and were not considered to have significantly altered the characteristics of the reinforcement. The construction details of the load cells and their calibration procedures can be found in Springman *et al.* [3]. The testing method consisted of first bringing the clay foundation to a state of hydrostatic pore pressure equilibrium. After the clay foundation reached pore pressure equilibrium by continuous swelling near the top and recompression near the bottom, the lateral effective stresses could be inferred using the known cycles of vertical effective stress and data of one-dimensional

consolidation and swelling for speswhite kaolin obtained by Al-Tabbaa [4]. Figure 3 shows these states of stresses. After achieving pore pressure equilibrium, in-flight vane shear tests were carried out at different depths. Figure 4 shows the undrained shear strength profile measured by in-flight vane shear tests. After carrying out vane shear tests, an embankment was placed in-flight in 20 stages (15 s time interval between successive stages) by pouring sand from a hopper mounted on the top of the strongbox.

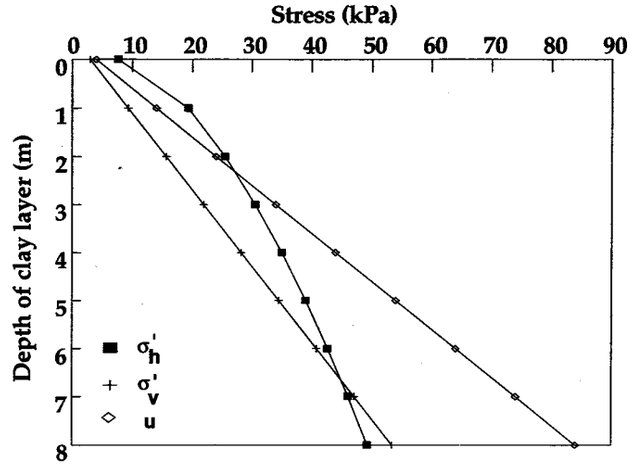

Fig. 3. Stress state of the clay foundation prior to embankment construction.

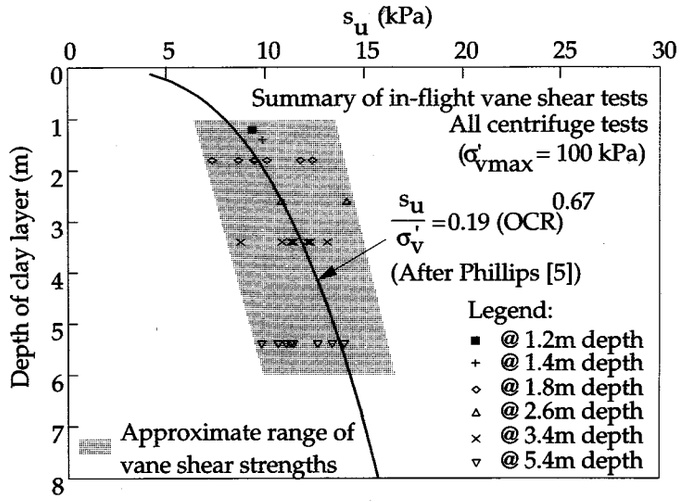

Fig. 4. Undrained shear strength profile of the clay foundation.

Rapid construction of the embankment caused significant deformation of the clay foundation. Excess pore pressures in the clay and the tension in the reinforcement both increased as the embankment construction progressed. The clay foundation for test JSS8 (unreinforced) failed when about 85% of the embankment was constructed. Lateral displacement up to 5 mm was recorded in the clay foundation at the end of embankment construction for test JSS7 (deep clay layer) whereas that for test JSS12 (shallow clay layer) was less than 1.5 mm. Figures 5 and 6, obtained by measuring the in-flight photographs taken before and immediately after embankment construction,

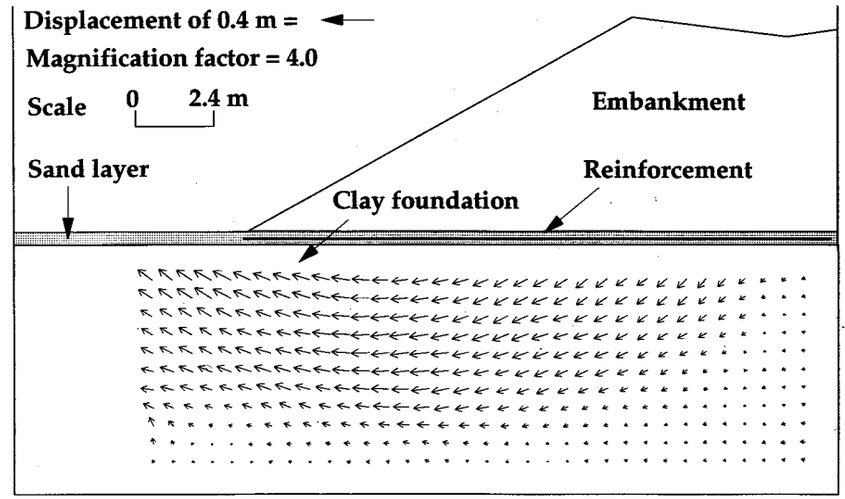

Fig. 5. Displacement of the clay foundation due to embankment construction (test JSS7, deep clay layer).

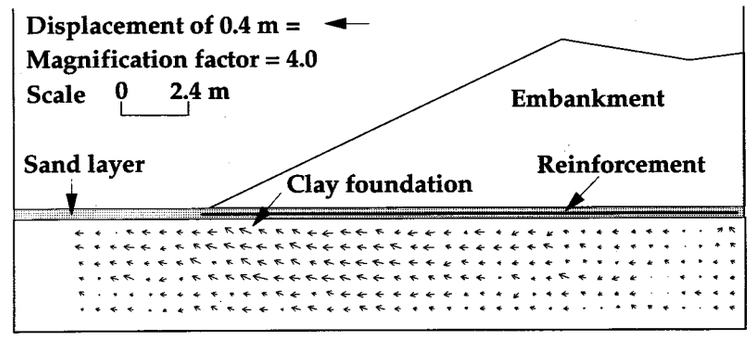

Fig. 6. Displacement of the clay foundation due to embankment construction (test JSS12, shallow clay layer).

show the displacement of clay foundation for tests JSS7 and JSS12. Maximum tension in the geotextile recorded at the end of embankment construction was 1.5 kN/m for test JSS7 and 0.7 kN/m for test JSS12.

The consolidation of the clay foundation was nearly completed in 6 h (400 days at prototype scale) for test JSS7 and in 1.5 h (100 days at prototype scale) for test JSS12. Ground movements due to consolidation were mainly one-dimensional and were concentrated underneath the embankment. There was a small reduction in the reinforcement tension for both the tests indicating that the critical phase for the embankment was just after the completion of its construction.

ANISOTROPIC BEHAVIOUR OF THE CLAY FOUNDATION

As with any other soil–structure interaction problem, modelling the behaviour of foundation soil is important when carrying out finite element analysis of reinforced embankments on soft clay. Experimental investigations into the properties of one dimensionally consolidated speswhite kaolin by several research workers (Al-Tabbaa [6], Atkinson *et al.* [7]) have shown that its yield locus is not symmetric about the p'- axis but has an inclined axis of symmetry in q–p' space, indicating stress-induced anisotropy (Fig. 7).

Accurate modelling of anisotropic behaviour of the clay foundation is very important in the analysis of embankments on soft clay. As shown in Fig. 8, the embankment loading causes rotation of principal stresses in clay from

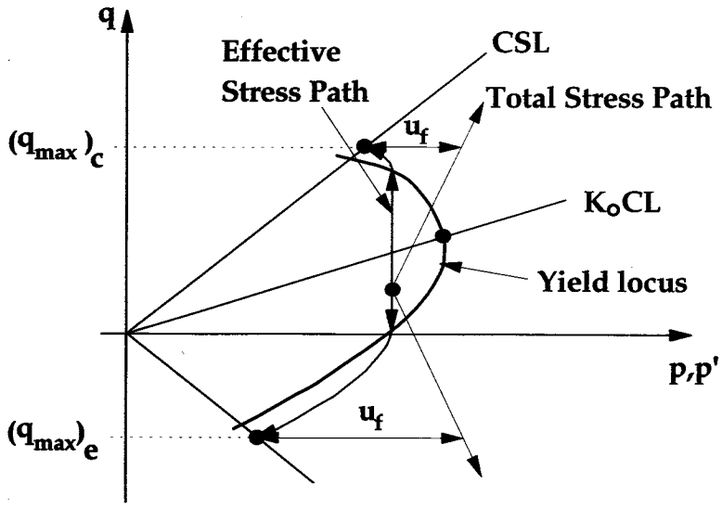

Fig. 7. Anisotropic yield locus for 1-*d* consolidated speswhite kaolin.

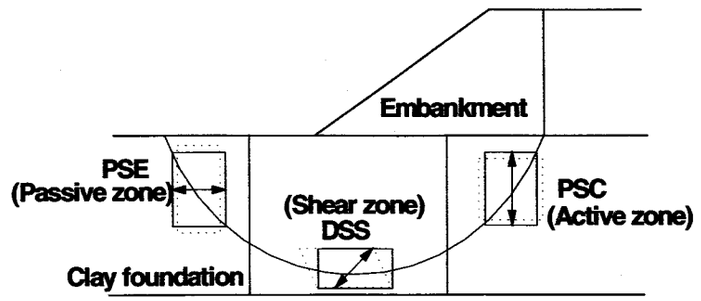

Fig. 8. Modes of deformation of the clay foundation due to embankment construction.

nearly vertical underneath the shoulder to nearly horizontal beyond the toe of the embankment. Experimental investigations by several research workers (Bjerrum [8], Kinner and Ladd [9], Ladd and Foott [10], Ohta *et al.* [11]) suggest that the undrained shear strength (S_u) of an anisotropically consolidated clay reduces as the direction of principal stress changes from nearly vertical in the active zone to nearly horizontal in passive zone. S_u in the passive zone can be almost half of that in the active zone.

The following equation, relating the ratio (K_s) of undrained shear strength obtained from a plane strain extension test and that obtained from a plane strain compression test and plasticity index (I_p) was suggested by Kulhawy and Mayne [12] based on large number of tests carried out on natural clays:

$$K_s = 0.35 + 0.0085 I_p \tag{1}$$

Substituting $I_p = 31$ for speswhite kaolin [13] in eqn (1), $K_s = 0.61$. Hence,

$$\left(\frac{s_u}{\sigma'_{v\,max}}\right)_{PSE} = 0.61\left(\frac{s_u}{\sigma'_{v\,max}}\right)_{PSC} \tag{2}$$

Prevost [14] developed the following simple relationship between undrained shear strengths of normally consolidated clay obtained from different tests:

$$\left(\frac{s_u}{\sigma'_{v\,max}}\right)_{DSS} = 0.45\left\{\left(\frac{s_u}{\sigma'_{v\,max}}\right)_{PSC} + \left(\frac{s_u}{\sigma'_{v\,max}}\right)_{PSE}\right\} \tag{3}$$

where the subscripts PSC, PSE and DSS stand for plane strain compression, plane strain extension and direct simple shear, respectively. Equation (3) is consistent with previous experimental observations (e.g. Ladd and Foott

[10]) that the undrained shear strength obtained from direct simple shear test is roughly equal to the average of the plane strain compression and extension strengths. Kulhawy and Mayne [12], plotted available undrained shear strength data for 42 intact clays and suggested the following equation:

$$\left(\frac{s_u}{\sigma'_{v\,max}}\right)_{DSS} = 0.40\left\{\left(\frac{s_u}{\sigma'_{v\,max}}\right)_{PSC} + \left(\frac{s_u}{\sigma'_{v\,max}}\right)_{PSE}\right\} \quad (4)$$

which is similar to the equation proposed by Prevost but has a lower regression coefficient. Combining eqns (2) and (4), the following relationship can be obtained:

$$\left(\frac{s_u}{\sigma'_{v\,max}}\right)_{DSS} = 0.644\left(\frac{s_u}{\sigma'_{v\,max}}\right)_{PSC} \quad (5)$$

Therefore, from eqns (2) and (5), it can be concluded that the ratio of undrained shear strength of an anisotropically consolidated clay in active, shear and passive zones is 1 : 0.644 : 0.61. It should, however, be emphasized that this ratio is obtained for normally consolidated clays. The undrained shear strength of overconsolidated clays depends on the OCR (overconsolidation ratio based on vertical effective stresses) and the undrained shear strength at OCR = 1 (normally consolidated state). Based on the experimental data of six different clays (taken from Ladd *et al.* [15]), Kulhawy and Mayne [12] have suggested the following relationship:

$$\frac{(s_u/\sigma'_v)_{OC}}{(s_u/\sigma'_{v\,max})_{NC}} = OCR^m \quad (6)$$

They suggested a value of 0.8 for m. It should be noted that the general form of eqn (6) will hold regardless of the test type [16]. However, the undrained shear strength ratio in a normally consolidated state will vary significantly as described above and the variation in m will be small. Hence, the ratio 1 : 0.644 : 0.61 for undrained shear strengths in active, shear and passive zones could well be applied for overconsolidated clays.

FINITE ELEMENT ANALYSES

A selected increment version of the finite element program CRISP [17], called CRISP93 and mounted on an IBM compatible personal computer, was used for the analyses. CRISP93 is specified in *Users' Manuals*, Vols 1 and 3 [18]. The following modifications were carried out to make CRISP93 more suitable for the analyses carried out in the present study:

(1) The formulation of bar elements was changed so that they could model a synthetic reinforcement more closely. The modified bar elements are bilinear elastic and they cannot take any compressive force.
(2) The formulation of the Schofield model was changed in such a way that the shear modulus G could be specified proportional to the mean effective stress p'. This modification implies that G is also a function of the stress history of the foundation since the magnitude of p' depends on the stress history. It is worth noting that the value of G is the same in all directions, i.e. anisotropic elasticity cannot be specified for the foundation if the Schofield model is used.
(3) The horizontal and vertical permeabilities were defined as functions of current void ratio based on the relationships suggested by Al-Tabbaa [4] for speswhite kaolin.

The geometry

Figure 9 shows the details of the meshes used for the analyses. They are 2-D plane strain meshes with boundary conditions similar to those of a typical centrifuge model with all dimensions 40 times those of the centrifuge model (simulating a full-scale prototype).

The clay foundation was modelled using 298 elements (64 linear strain triangles and 234 linear strain quadrilaterals with displacements and pore pressures unknown) for analyses with 8 m deep clay foundation and using 230 elements (linear strain quadrilaterals with displacements and pore pressures unknown) for analyses with 4 m deep clay foundation. The sand embankment was modelled using 253 elements (187 linear strain triangles and 66 linear strain quadrilaterals with displacements unknown). These were added in-place in seven layers to simulate the construction of the sand embankment in-flight in the centrifuge model tests (Fig. 10). The shape of each of the seven layers was derived from in-flight photographic measurements. The time allowed for the construction of each layer was proportional to its area, i.e. the rate of construction was linear. The reinforcement was modelled using 22 modified bar elements. The clay–reinforcement and sand–reinforcement interfaces were modelled using 44 interface elements.

Material modelling

(a) Clay foundation

It has been shown in the past that good agreement can be reached between the experimental results and numerical predictions when speswhite kaolin is

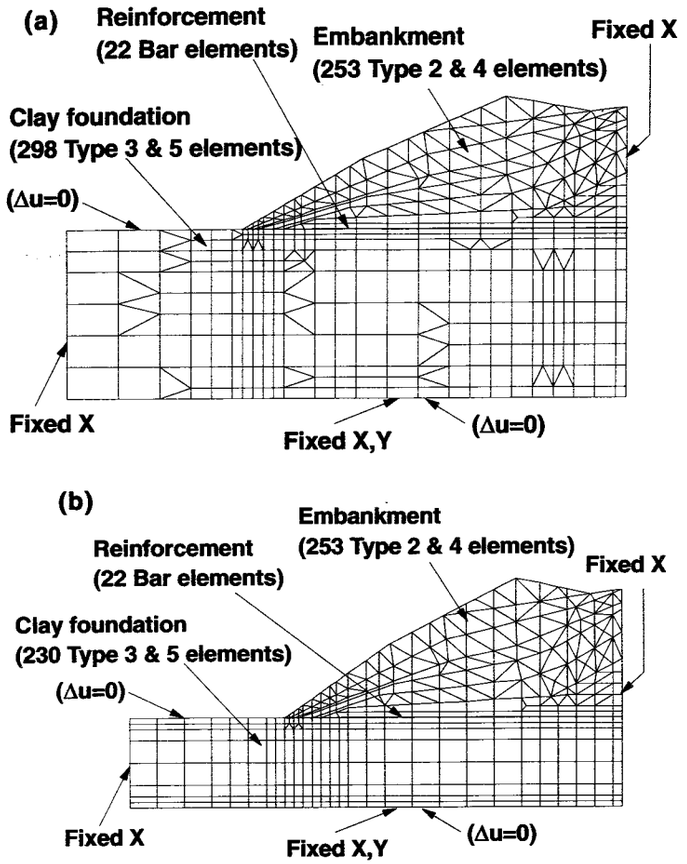

Fig. 9. The finite element meshes.

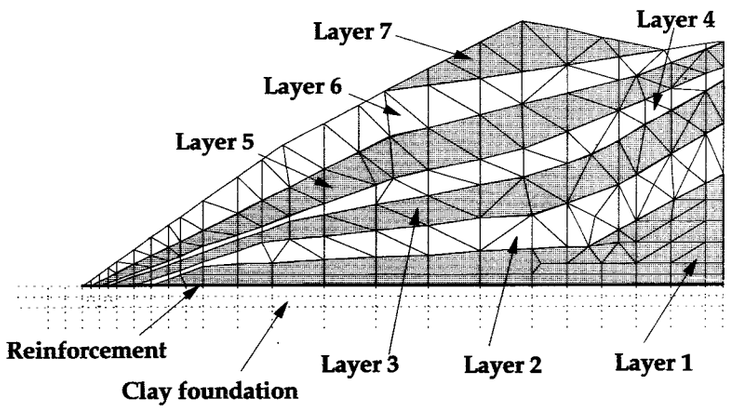

Fig. 10. Staged building of elements to simulate embankment construction.

modelled using critical state models [19, 20]. However, the critical state models in CRISP93 assume the soil to be isotropic, and hence cannot model the anisotropic behaviour of kaolin described in Section 3. In the analyses presented here, an attempt was made to model the anisotropic behaviour using the Schofield model (Fig. 11).

The Schofield model was chosen because the clay foundation was heavily overconsolidated at the top with OCR ranging from 33 at the surface to around 4 at 3 m depth. The mesh representing the clay foundation was divided into three zones as shown in Fig. 12. In the zone entirely underneath the embankment, the mode of deformation was assumed to be active (plane strain compression) whereas in the zone farthest from the embankment, it

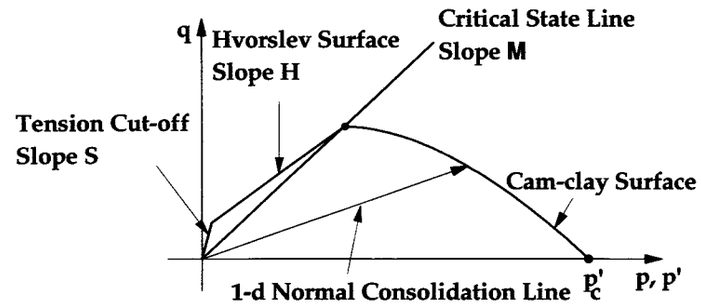

Fig. 11. Yield surface of the Schofield model.

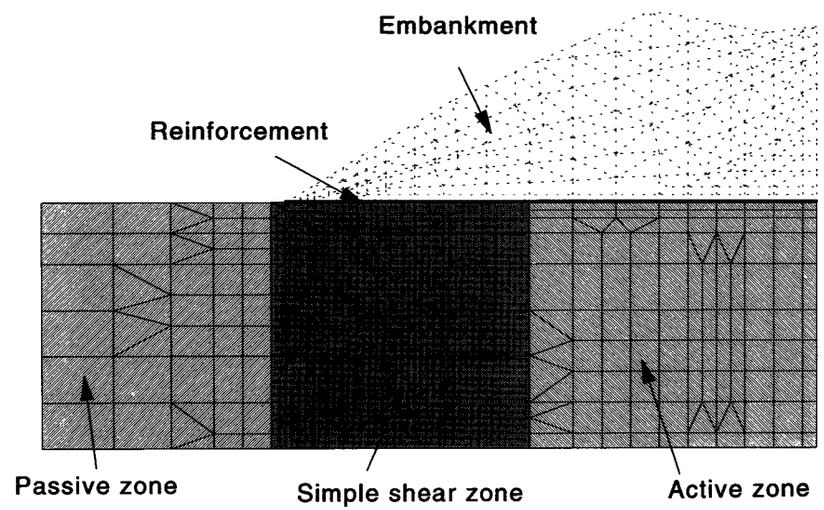

Fig. 12. Idealized zones in the clay foundation.

was assumed to be passive (plane strain extension). For the zone in the middle, plane strain simple shear mode of deformation was assumed.

Based on the arguments presented in Section 3, the ratio of S_u in these three zones was specified as 1 (active) : 0.644 (shear) : 0.61 (passive). This can be achieved in two ways: (1) by reducing the respective values of M (slope of CSL in q–p' space) in the shear and passive zones to 0.644 and 0.61 times the value of M in the active zone, and (2) by reducing the respective values of p'_c (max. preconsolidation pressure) in the shear and passive zones to 0.592 and 0.559 times the value of p'_c in active zone. The first approach was rejected on the basis of the observation that same value of the critical state angle of internal friction is obtained in both the triaxial compression and triaxial extension tests on speswhite kaolin [4, 21] which gives the same value of M in plane strain compression and extension assuming ideal plasticity [22]. Hence, following the second approach, $p'_c = 133$ kPa was specified in the active zone based on $K_{ONC} = 0.69$ [4] and $\sigma'_{vmax} = 100$ kPa. It was reduced to 78.7 kPa in the shear zone and 74.3 kPa in the passive zone. Most of the critical state parameters for the clay foundation were derived from Al-Tabbaa [4]. Table 2 lists all the parameters specified for clay foundation.

(b) Sand embankment

The sand embankment was modelled using an elastic–perfectly plastic model with the Mohr–Coulomb yield criterion. A critical state angle of internal friction was used for unreinforced embankments since large strains were anticipated at latter stages of analysis, whereas a peak angle of internal friction was used for reinforced embankments since small strains were expected throughout the analysis. A small value of apparent cohesion $c' = 1$ kPa was specified in order to avoid numerical instabilities near the toe of the embankment. The average bulk unit weight (γ) of sand in the embankment as poured during centrifuge testing was 17.1 kN/m^3. However, γ was reduced to 16 kN/m^3 in order to compensate for the friction estimated to occur between the sand and the inner sides of the strongbox. The estimation of friction was based on the coefficients of friction obtained by Waggett [23] for sand–perspex and sand–polished steel interfaces. The elastic stiffness for

TABLE 2
Parameters for the clay foundation

κ	λ	Γ	M	ν	γ	H	S
0.028	0.187	3.00	0.756	0.3	16.3	0.59	2.00

where H is the slope of the Hvorslev surface in V–p'–q space and S is the slope of the tension cut-off surface.

each of the seven layers were specified as shown in Table 3. It was highest for the lowermost layer and was lowest for the topmost layer. However, it has been pointed out by Kwok [24] that elastic stiffness of the embankment material has little influence on the overall behaviour of reinforced embankment as predicted by finite element analyses. Kwok's [24] inference was based on the observation that his sand embankment modelled by an elastic–perfectly plastic model yielded almost everywhere for each layer at the end of its construction which would indicate that the dominant strains in the embankment were the plastic strains and not the elastic strains. Therefore, no testing was undertaken to derive the elastic stiffness of the sand embankment and the values input in the analyses are approximate. Table 4 lists all the parameters specified for the sand embankment.

(c) Reinforcement

The reinforcement was modelled using bi-linear elastic bar elements having no compressive strength. The stiffness of the reinforcement was derived from load-elongation curves obtained by carrying out 1%/min tensile tests on 200 mm wide strips of the reinforcement. Table 5 gives all the parameters specified for the reinforcement. It should be noted that the axial stiffness of a

TABLE 3
Elastic stiffness of different layers of the embankment

Layer No.	*1*	*2*	*3*	*4*	*5*	*6*	*7*
Young's modulus (kPa)	10000	8500	7650	6850	6000	5300	4500

TABLE 4
Parameters for the sand embankment

ν'	c' (kPa)	ϕ'_{CRIT}	ϕ'_{PEAK}	γ(kN/m^3)
0.3	1.0	35°	50°	16.0

TABLE 5
Parameters for the reinforcement

E_1(kPa)	E_2(kPa)	ϵ_t(%)	A_r(m^2/m)	ν
1,700,000	2,700,000	0.6	0.00212	0.35

Where E_1 is Young's modulus of the reinforcement up to the threshold strain (ϵ_t) and E_2 is Young's modulus of the reinforcement beyond ϵ_t.

geotextile or a geogrid is usually expressed as force per unit width per unit strain (kN/m), commonly referred to as the modulus of the reinforcement. In the formulation of bar elements in CRISP93, the modulus of reinforcement is equal to its Young's modulus (E) multiplied by the area per metre width (A_r). The area per metre width of the reinforcement was taken equal to 0.00212 m^2/m based on Springman *et al.* [3].

(d) Soil–reinforcement interfaces

Both the clay–reinforcement and the sand–reinforcement interfaces were modelled using nodal compatibility slip elements. These slip elements were assigned a stiffness similar to the adjacent soil elements and the yielding was controlled by Mohr–Coulomb strength parameters c and ϕ. Since the reinforcement was installed at the top drainage boundary, effective stress parameters were used for the interfaces. These parameters are listed in Table 6.

Outline of the analyses

Four analyses were carried out. Table 7 gives brief description of these analyses. For all these analyses, the embankment construction was carried out in seven stages (one layer per stage). The total time allowed for embankment construction was 6.11 days. After the construction, the clay foundation was allowed to consolidate for 518 days under the embankment loading.

TABLE 6
Parameters for soil–reinforcement interfaces

Interface	c' *(kPa)*	$\phi'(°)$	k_n*(kPa)*	k_s*(kPa)*	k_{sres}*(kPa)*	t*(m)*
Clay–reinforcement	0.0	25.8	3500	1000	10	0.04
Sand–reinforcement	0.0	35	13000	3800	40	0.04

where k_n is the normal stiffness, k_s is the shear stiffness, k_{sres} is the residual shear stiffness and t is the thickness of the interface elements.

TABLE 7
Details of the finite element analyses

Analysis	*Test code*	*Details*
U8FASTI	JSS8	Isotropic clay foundation (p'_c = 133 kPa throughout the clay foundation)
U8FASTA	JSS8	Anisotropic clay foundation
R8GTX	JSS7	Geotextile, deep clay foundation
R4GTX	JSS12	Geotextile, shallow clay foundation

The results

(a) Collapse height of unreinforced embankment

Figure 13 shows the horizontal displacement of node 136 (located in the mesh representing the clay foundation) as predicted by analyses U8FASTI and U8FASTA. As mentioned above, during centrifuge test JSS8, the clay foundation failed when 85% of the embankment was constructed. It is clear from Fig. 13 that analysis U8FASTA, which incorporated the anisotropic behaviour of clay foundation, predicted the collapse height of the embankment reasonably well. Up to 30% deviatoric strains were observed in the embankment for analysis U8FASTA. Hence, the use of the critical state angle of internal friction in this analysis is justified. After the approximate approach of modelling the anisotropic behaviour of foundation soil was successfully calibrated in this way, it was used for the analyses involving reinforced embankments

(b) Excess pore pressures in clay

Figure 14 shows the comparison between the measured and predicted excess pore pressures in clay at two different locations as predicted by analyses R8GTX and R4GTX. Table 8 gives the summary of measured and predicted excess pore pressures at seven different pore pressure transducer locations (see Fig. 2).

From Fig. 14 and Table 8, it can be seen that the analyses predicted the magnitude of excess pore pressures during embankment construction fairly accurately almost everywhere except in the passive zone for the unreinforced

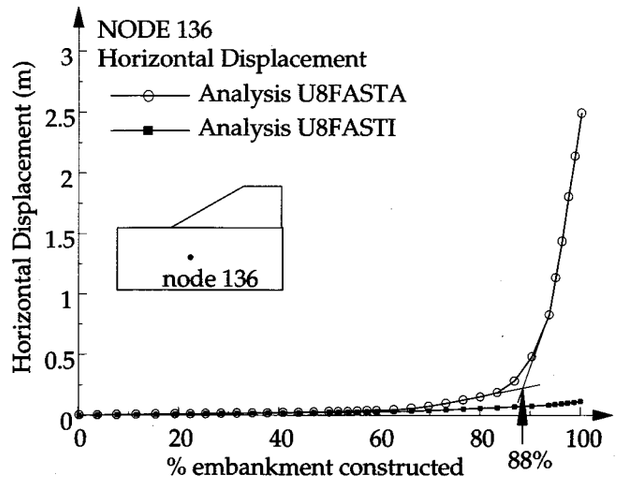

Fig. 13. Prediction of collapse height of unreinforced embankment.

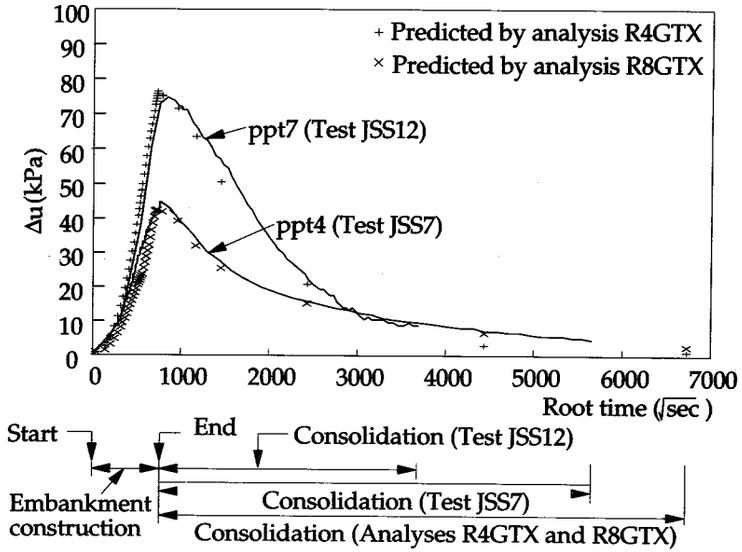

Fig. 14. Measured and predicted excess pore pressures.

TABLE 8
Magnitudes of measured and predicted peak excess pore pressures (kPa)

PPT position →	*1*	*2*	*3*	*4*	*5*	*6*	*7*
Test JSS8	33	24	29	42	—	70	—
U8FASTA	13	20	27	32	40	55	47
Test JSS7	—	24	33	45	49	64	65
R8GTX	10	19	25	43	38	54	55
Test JSS12	2	7	18	44	44	34	77
R4GTX	4	5	14	37	39	39	77

case where they were underpredicted. However, it should be noted that ppt location 1 was in close proximity of the in-flight vane shear test sites and that these vane shear tests might have contributed towards the excess pore pressures measured at that location. Treating the permeability of the clay foundation as a function of its void ratio has resulted in excellent prediction of the dissipation of excess pore pressures after the end of embankment construction, as seen from Fig. 14. It is worth noting that specifying a constant value of permeability for the clay foundation may result in significant overprediction of the rate of consolidation (e.g. Russell [22] and Almeida [25]) both during and after the embankment construction.

(c) Displacement of clay foundation

Figure 15 shows the measured and predicted settlements of the top of clay foundation for the reinforced cases. The measured and predicted horizontal displacement of clay foundation at two "inclinometer" locations (each consisting of a column of black markers) are shown in Fig. 16. It can be seen from Fig. 15 that the settlements were well-predicted almost everywhere except near the right-hand side boundary where they were underpredicted. The measured settlements near the RHS boundary might have been less due to the presence of clamp for the geotextile.

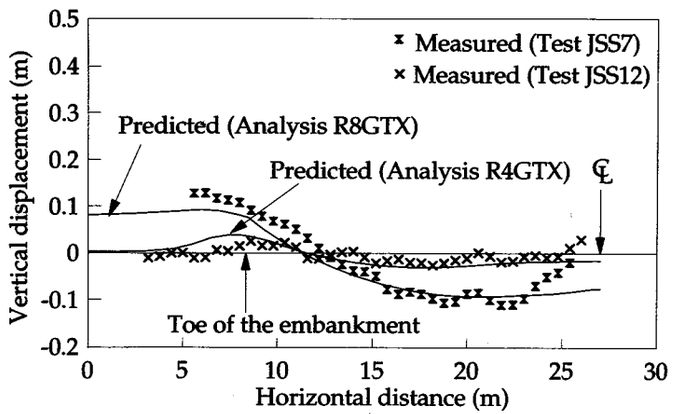

Fig. 15. Measured and predicted settlements (analyses R8GTX and R4GTX).

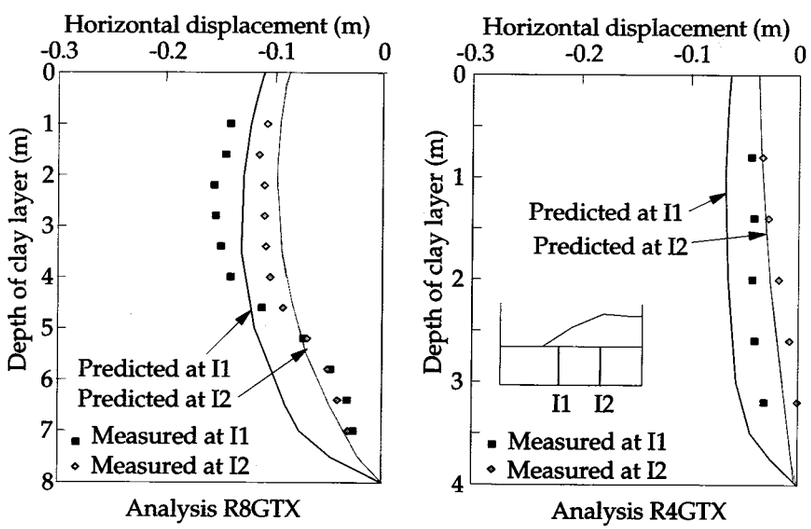

Fig. 16. Horizontal displacements of the clay foundation.

The horizontal displacements were reasonably well-predicted underneath the embankment for the shallow clay layer but were overpredicted away from the embankment. For the deep clay layer, the horizontal displacements were underpredicted in the top half of the clay foundation but were well-predicted in the bottom half. This may be due to the fact that in test JSS7 (deep clay layer) the top half of the clay came into pore pressure equilibrium by continuous swelling. Therefore, when the embankment was constructed, the clay in the passive zone continued to swell, i.e. the direction of the stress path did not change which resulted in a lower stiffness of clay foundation in the passive zone compared to that in the active zone in which there was a reversal of stress path. This might have resulted in higher lateral deformation of the top half of the clay foundation. Such modelling of soil stiffness based on the direction of loading was not possible using the Schofield or any other soil model present in the version of CRISP used.

(d) Tension in the reinforcement

Figure 17 shows the measured and predicted tension profiles for the reinforced cases. As seen from Fig. 17, the tension profile was well-predicted for the shallow clay layer (test JSS12 and analysis R4GTX). For the deep, clay layer case (test JSS7 and analysis R8GTX), the maximum tension in the reinforcement was well-predicted but the tension underneath the slope of the embankment was underpredicted. The reason for this may be the same responsible for the underprediction of lateral deformation of clay.

Also, the magnitude of tension induced in the reinforcement is very sensitive to the variation in the undrained shear strength of the clay foundation as seen from Fig. 18 showing the tension profiles predicted by analysis R8GTX.

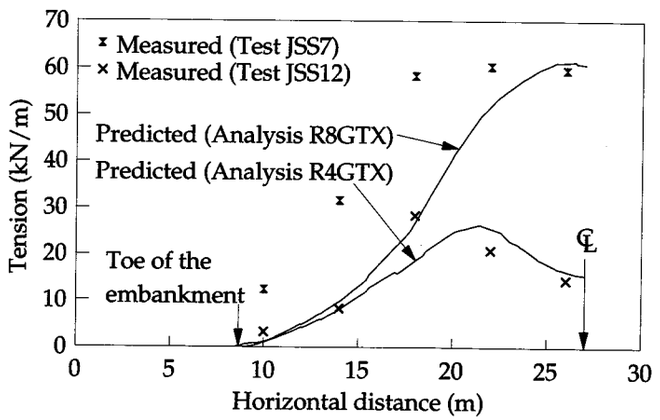

Fig. 17. Measured and predicted tension in the reinforcement.

Profile 1 is predicted by analysis A with σ'_{vmax} = 100 kPa (p'_c = 133 kPa in the active zone) for the clay foundation whereas profile 2 is predicted by analysis B with σ'_{vmax} = 90 kPa (p'_c = 120 kPa in the active zone). The undrained shear strength of the clay for analysis B is only 8.4% less than that for analysis A whereas the magnitude of maximum tension predicted by analysis B is 67% more than that predicted by analysis A.

(d) Effectiveness of the reinforcement

Figure 19 shows the contours for stress ratio η (q / p') for the analysis R8GTX at the end of embankment construction. As seen from Fig. 19, almost the entire clay foundation has a stress ratio between 0.7 and 0.8 which is quite close to the slope of the critical state line in q–p' space (M = 0.756). Therefore, at the end of embankment construction, almost the entire clay foundation is at critical state. Yet, the embankment remains stable. At this stage, it is only the reinforcement that is preventing the failure of embankment.

Conclusions

The approximate modelling of stress-induced anisotropy of 1-d consolidated clay foundation was successful in predicting the overall behaviour of unreinforced and reinforced embankments. The collapse height of an unreinforced embankment was reasonably well-predicted. Predictions of excess pore pressures, settlements and lateral deformations of clay foundation were in good agreement with the measured values for all the analyses.

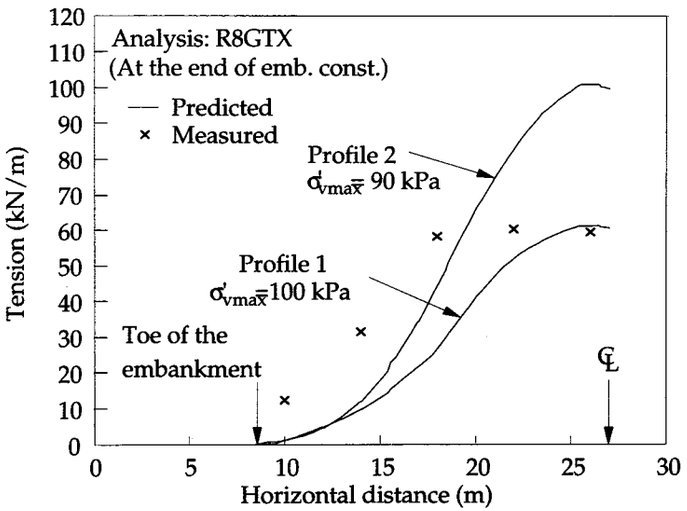

Fig. 18. Influence of the strength of the clay on tension induced in the reinforcement.

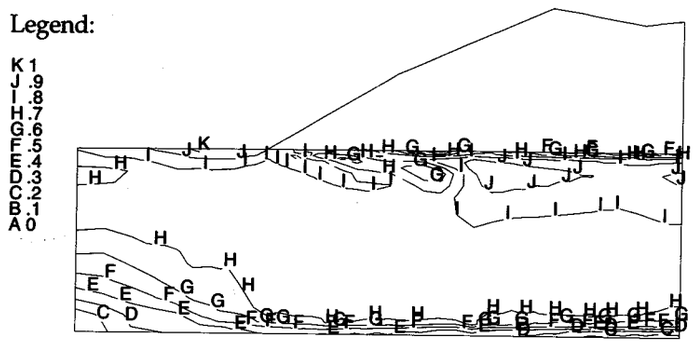

Fig. 19. Contours of stress ratio η (analysis R8GTX).

Measured and predicted tensions in the reinforcement were also in close agreement. Although the tension mobilized in the reinforcement is found to be only of the order of lateral thrust in the embankment, it can be very effective in improving the short-term stability of the embankment in situations where the factor of safety is slightly less than one. The tension in the reinforcement is sensitive to the magnitude and distribution of shear strength of clay foundation. Hence, in order to accurately model the overall behaviour of reinforced embankment on soft clay, it is important to correctly model the behaviour of the clay foundation. The use of a constitutive model which accounts for the induced anisotropy would surely be more scientific and objective. However, if the finite element code does not have such a model, the approximate approach suggested in this paper makes it possible to model the overall behaviour of reinforced embankments on soft clay fairly accurately. The suggested approximate approach is based on several experimental evidences of reduction in undrained shear strength in intact and remoulded clays exhibiting stress-induced anisotropy and there is no reason why it cannot be used in other similar field situations. However, its use may not be feasible in situations where the subsoil profile is very complicated or it consists of soils having peculiar properties (e.g. organic soils).

ACKNOWLEDGEMENTS

Jitendra Sharma is grateful for the financial support of the Nehru Trust for Cambridge University and the ORS award given by the CVCP of British University for his Ph.D. study at Cambridge University.

The views expressed in this paper are not necessarily of the Department of Transport. Extracts from this text may be reproduced except for commercial purposes, provided that the source is acknowledged. The work described here forms part of the programme of Transport Research Laboratory and this paper is published by the permission of its chief executive.

REFERENCES

1. Schofield, A. N., Cambridge University geotechnical centrifuge operations. *Géotechnique*, **30** (1980) 227–268.
2. Sharma, J. S., Behaviour of reinforced embankments on soft clay. Ph.D. dissertation, Cambridge University 1994.
3. Springman, S. M., Bolton, M. D., Sharma, J. S., & Balachandran, S., Modelling and instrumentation of a geotextile in the geotechnical centrifuge. *Proc. Int. Symp. on Earth Retaining Practice*, Kyushu, pp. 167–172, 1992.
4. Al-Tabbaa, A., Permeability and stress–strain response of speswhite kaolin. Ph.D. dissertation, Cambridge University, 1987.
5. Phillips, R., Centrifuge lateral pile tests in clay: Tasks 2 & 3. A report to Exxon Product Research Corporation by Lynxvale Ltd, Cambridge, U.K., 1988.
6. Al-Tabbaa, A., Anisotropy of clay. M. Phil. dissertation, Cambridge University, 1984.
7. Atkinson, J. H., Richardson, D., & Robinson, P. J., Compression and extension of K_o normally consolidated kaolin clay. *J. Geotech. Engng Div., ASCE*, **113** (1987) 1468–1482.
8. Bjerrum, L., Embankments on soft ground. In *Performance of Earth and Earth-Supported Structures — Proc. ASCE Speciality Conference*, Vol. 2, pp 1–54, 1972.
9. Kinner, E. B. & Ladd, C. C., Undrained bearing capacity of footings on clay. *Proc. 8th ICSMFE*, Moscow, Vol. 1, pp. 209–215, 1973.
10. Ladd, C. C. & Foott, R., New design procedure for stability of soft clays *J. Geotech. Engng Div., ASCE*, **100** (1974) 763–786.
11. Ohta, H., Nishihara, A., & Morita, A., Undrained stability of K_o consolidated clays. *Proc. 11th ICSMFE*, San Francisco, Vol. 2, pp. 613–617, 1985.
12. Kulhawy, F. H. & Mayne, P. W., Manual on estimating soil properties for foundation design, EPRI EL-6800, Project 1493-6. Final report prepared by Cornell University, Ithaca, NY.
13. Airey, D. W., Clays in circular simple shear apparatus. Ph.D. dissertation, Cambridge University, 1984.
14. Prevost, J. H., Undrained shear tests on clays. *J. Geotech. Engng Div. ASCE*, **105** (1979) 49–64.
15. Ladd, C. C., Foott, R., Ishihara, K., Schlosser, F., & Poulos, H. G., Stress-deformation and strength characteristics. *Proc. 9th ICSMFE*, Tokyo, Vol. 2, pp. 421–494, 1977.
16. Wroth, C. P., Interpretation of *in-situ* soil tests. *Géotechnique*, **34** (1984) 449–489.
17. Britto, A. M. & Gunn, M. J., *Critical State Soil Mechanics via Finite Elements*. Horwood, Chichester, 1987.
18. Britto, A. M. & Gunn, M. J., *CRISP90 — User's and Programmer's Guide*, Vols 1 and 3. Cambridge University Engineering Department, 1990.

19. Kusakabe, O., Stability of excavations in soft clay. Ph.D. dissertation, Cambridge University, 1982.
20. Phillips, R., Ground deformation in the vicinity of a trench heading. Ph.D. dissertation, Cambridge University, 1987.
21. Stewart, D. I., Groundwater effects on *in-situ* walls in stiff clays. Ph.D. dissertation, Cambridge University, 1989.
22. Russell, D., Finite element analysis of embankments on soft ground incorporating reinforcement and wick drains. Ph.D. dissertation, University of Sheffield, 1992.
23. Waggett, P., The effect of lubricants on the interaction between soils and perspex. Part 2 Project Report, Cambridge University Engineering Department, 1987.
24. Kwok, C. M., Reinforced embankments on soft ground. Ph.D. dissertation, University of Sheffield, 1987.
25. Almeida, M. S. S., Stage constructed embankments on soft clays. Ph.D. dissertation, Cambridge University, 1984.